DALTON
FULL PAPER

Diruthenium complexes with hydrotris(1-pyrazolyl)borate face-capping ligands involving $\{Ru_2(\mu\text{-O or }\mu\text{-OH})(\mu\text{-carboxylato})_2\}$ cores †

Tomoaki Tanase,*[a] Nao Takeshita,[a] Chiharu Inoue,[a] Merii Kato,[a] Shigenobu Yano[a] and Kiyoshi Sato[b]

[a] *Department of Chemistry, Faculty of Science, Nara Women's University, Kitauoya-higashi-machi, Nara 630-8285 Japan. E-mail: tanase@cc.nara-wu.ac.jp*
[b] *Department of Applied Chemistry, Faculty of Engineering, Tokyo Metropolitan University, 1-1 Minami-Ohsawa, Hachioji, Tokyo 192-0397, Japan*

Received 9th February 2001, Accepted 22nd May 2001
First published as an Advance Article on the web 6th July 2001

Reactions of $[Ru_2(RCOO)_4Cl]$ (R = Me, Ph) with $K[HBpz_3]$ ($HBpz_3^-$ = hydrotris(1-pyrazolyl)borate) afforded the oxo-bridged diruthenium(III) complexes, $[Ru_2(\mu\text{-O})(\mu\text{-RCOO})_2(HBpz_3)_2]$ (R = Me (**1a**), Ph (**1b**)) in moderate yields. Complexes **1** were converted by treatment with HPF_6 into the hydroxo-bridged diruthenium(III) complexes, $[Ru_2(\mu\text{-OH})(\mu\text{-RCOO})_2(HBpz_3)_2](PF_6)$ (R = Me (**2a**), Ph (**2b**)), and by reaction with $(NH_4)_2Ce(NO_3)_6$, to the oxo-bridged mixed-valence diruthenium(III, IV) complexes, $[Ru_2(\mu\text{-O})(\mu\text{-RCOO})_2(HBpz_3)_2](PF_6)$ (R = Me (**3a**), Ph (**3b**)). Complexes **1**–**3** were characterized by elemental analysis, IR, UV-Vis, and ^1H NMR spectroscopies, and X-ray absorption and crystallographic analyses (**1a** and **2a**). Complex **1a** consists of a $\{Ru_2(\mu\text{-oxo})(\mu\text{-carboxylato})_2\}$ core with two terminal face-capping $HBpz_3^-$ ligands (Ru · · · Ru = 3.2544(7) Å). Protonation of the μ-oxo group of **1a** expanded the Ru · · · Ru distance to 3.4490(9) Å, which was elucidated by X-ray crystallography, and one-electron oxidation of **1a** also increases this length to 3.38 Å, determined by EXAFS analysis. These complexes interestingly showed, in cyclic voltammograms, a wide range of redox processes, $[Ru^{II}_2] \leftrightarrow [Ru^{II}Ru^{III}] \leftrightarrow [Ru^{III}_2] \leftrightarrow [Ru^{III}Ru^{IV}] \leftrightarrow [Ru^{IV}_2]$, which are coupled with protonation/deprotonation at the monoatom bridge. When complex **1b** was reduced with sodium amalgam, the mononuclear ruthenium(II) complex $[Ru(PhCOO)(HBpz_3)(CH_3CN)_2]$ (**4b**) was isolated and characterized by spectroscopic techniques and EXAFS analysis. Upon exposure to air or dioxygen, complex **4b** readily regenerated the oxo-bridged dimer **1b**, and the oxo atom was confirmed to be derived from dioxygen by an isotopically-labeled experiment. The present results demonstrate the versatile redox states of diruthenium centres terminally capped by $HBpz_3^-$ ligands.

Introduction

Extensive biological and bioinorganic studies have been carried out on the non-heme diiron proteins, such as hemerythrin, the R2 subunit of ribonucleotide reductase, and methane monooxygenase, all of which involve diiron active centres bridged by carboxylates and a mono-atomic (oxo or hydroxo) bridging unit and function by utilizing redox cycles coupled with dioxygen molecules.[1–3] A number of synthetic models with a (μ-oxo, -hydroxo, or -alkoxo)bis(μ-carboxylato)diiron(III) core have already been reported,[1–3] but those involving higher valent Fe(IV) centres have not been studied in detail, owing to their instability, in spite of their biorelevant importance. We have been interested in the parallel chemistry of (μ-oxo, -hydroxo, or -alkoxo)bis(μ-carboxylato)diruthenium complexes, hoping to obtain detailed structural and physical information on a wide variety of oxidation states from $Ru(II)_2$ to $Ru(IV)_2$ and to utilize their redox properties to mimic biological systems and to develop catalytic organic reactions.[4,5]

Although the variety has been limited in comparison with that of diiron model complexes, many diruthenium(III) complexes involving the (μ-oxo)bis(μ-carboxylato)diruthenium core have been prepared and characterized.[6–12] In contrast, complexes with (μ-hydroxo)-, (μ-alkoxo)-, and (μ-phenoxo)-bis(μ-carboxylato)diruthenium(III) cores have been extremely limited. No detailed crystallographic study has been performed on (μ-hydroxo)bis(μ-carboxylato)diruthenium(III) complexes, and only three examples of the {(μ-alkoxo or -phenoxo)-bis(μ-carboxylato)diruthenium(III) complexes, $[Ru_2(\mu\text{-OMe})(p\text{-}OMeC_6H_4COO)_3(1\text{-MeIm})_4](PF_6)_2$ (1-MeIm = 1-methylimidazole),[13] $[Ru_2(\mu\text{-dhpta})(\mu\text{-}CH_3COO)_2]^-$ (H_5dhpta = 1,3-diamino-2-hydroxypropanetetraacetic acid),[4] and $[Ru_2(\mu\text{-hxta})(\mu\text{-PhCOO})_2]^-$ (H_5hxta = 2-hydroxy-5-methyl-*m*-phenylenedimethylenedinitrilotetraacetic acid),[5] have been reported. The (μ-oxo)bis(μ-carboxylato)diruthenium(III) complexes readily underwent one-electron oxidation and were converted into mixed-valence diruthenium(III, IV) complexes.[6,11] High valent oxo-bridged diruthenium(IV) complexes could also be useful artificial model systems for the oxygen evolving centre of photosystem II.[14,15] Alternatively, the diruthenium-(II, III)[16] and -(II, II)[17] complexes containing $\{(\mu\text{-}H_2O)(\mu\text{-RCOO})_2Ru_2\}$ cores have been established by using different terminal ligand systems including phosphines and dienes. This indicated the possibility that the choice of terminal ligand dramatically changes the redox properties of the triply bridged diruthenium centres.

Hydrotris(1-pyrazolyl)borate and its derivatives are known to stabilize relatively low valent metal centres acting as a six-electron-donor face capping ligand like cyclopentadienyl, and they also have the ability to cap oxidized metal centres.[18] In fact, interconversion of $Cu(I)_2$ to $Cu(II)_2$ and $Fe(II)_2$ to $Fe(III)_2$ by dioxygen have successfully been organized by using 3,5-dialkyl

† Electronic supplementary information (ESI) available: X-ray absorption spectra of **1a**, **2a**, **3a**, **1b**, **2b**, **3b**, **4b**; theoretical curve fitting results of **1a**, **2a**, **3a**, **1b**, **2b**, **3b**, **4b**; raw EXAFS of **1a**, **2a**, **3a**, **1b**, **2b**, **3b**, **4b**; ^1H–^1H COSY spectra of **2a**, **2b**. See http://www.rsc.org/suppdata/dt/b1/b101315g/

DOI: 10.1039/b101315g

substituted hydrotris(1-pyrazolyl)borate ligands.[19] In the present study, we have introduced hydrotris(1-pyrazolyl)borate ($HBpz_3^-$) as a terminal ligand, and wish to report herein the syntheses and structures of (μ-oxo or -hydroxo)bis(μ-carboxylato)diruthenium(III) complexes with $HBpz_3^-$ ligands, which afford a wide range of oxidation states *via* protonation and deprotonation of the mono-atom bridge. A preliminary result has already been reported.[20]

Experimental

All reagents were of the best commercial grade and were used without further purification. $[Ru_2(RCOO)_4Cl]$ (R = Me, Ph)[21,22] and potassium hydrotris(3,5-dimethyl-1-pyrazolyl)borate ($K[HB(3,5\text{-}Me_2pz)_3]$)[23] were prepared by known methods. Potassium hydrotris(1-pyrazolyl)borate ($K[HBpz_3]$) was purchased from Acros Co. Ltd.

Measurements

^1H and ^1H–^1H COSY NMR spectra were measured on a Varian Gemini2000 instrument at 300 MHz in $CDCl_3$. Chemical shifts were calibrated to $SiMe_4$ as an internal reference. Infrared absorption spectra were recorded with Jasco FT/IR-5300 and FT/IR-400 spectrometers. Electronic absorption spectra (UV-Vis) were measured on a Shimadzu UV3100 spectrometer. Mass spectra were measured on a JEOL LX-1000 spectrometer (FAB mode) by using nitrobenzoyl alcohol matrix. Cyclic voltammograms were measured with a BAS CV-50W Voltammetric Analyzer by using a conventional three electrode system, glassy carbon (working electrode), platinum wire (counter electrode), and $Ag/AgPF_6$ (in acetonitrile) reference electrode. Coulometric analysis was carried out with the same instrument by using a mercury-pool working electrode.

Preparation of complexes

$[Ru_2(\mu\text{-}O)(\mu\text{-}RCOO)_2(HBpz_3)_2]$ (R = Me (1a), Ph (1b)). $[Ru_2(CH_3COO)_4Cl]$ (502 mg, 1.06 mmol) and $K[HBpz_3]$ (534 mg, 2.12 mmol) were dissolved in 30 mL of methanol and the solution was stirred at room temperature for 12 h. The reaction mixture was concentrated and chromatographed on an alumina column (10% deactivated) (2.5 cm × 15 cm) eluted with CH_2Cl_2. The blue major band was collected and concentrated to dryness. The residue was crystallized from hot ethanol to give microcrystals of $[Ru_2(\mu\text{-}O)(\mu\text{-}CH_3COO)_2(HBpz_3)_2]\cdot EtOH$ (**1a**·EtOH) in 54% yield. Anal. Calcd for $C_{24}H_{32}N_{12}O_6Ru_2B_2$: C, 35.65; H, 3.99; N, 20.79. Found: C, 35.31; H, 4.04; N, 21.05%. IR (KBr): *ν* 2477m, 1550s, 1499m, 1418s, 1313s, 1211s, 1114s, 1049s, 792m, 756s, 715s, 621m cm^{-1}. UV-Vis (in acetonitrile): λ_{max} (*ε*) 570 (13.94), 276 (19.38) nm (10^3 M^{-1} cm^{-1}). ^1H NMR (in $CDCl_3$): *δ* 1.82 (s, $MeCO_2$, 6H), 5.50 (s, pz, 4H), 6.07 (s, pz, 4H), 7.01 (s, pz, 2H), 7.84 (s, pz, 4H), 8.62 (s, pz, 2H), 8.82 (s, pz, 2H). A slow vapor diffusion of Et_2O into a concentrated CH_2Cl_2 solution of **1a**·EtOH gave block shaped crystals of **1a**·Et_2O which were suitable for X-ray crystallography.

$[Ru_2(PhCOO)_4Cl]$ (220 mg, 0.30 mmol) and $K[HBpz_3]$ (155 mg, 0.62 mmol) were dissolved in 20 mL of methanol and the solution was stirred at room temperature for 5 h. The reaction mixture was concentrated and chromatographed on an alumina column (10% deactivated) (2.5 cm × 10 cm) eluted with CH_2Cl_2. The blue major band was collected and concentrated to *ca.* 4 mL. After addition of Et_2O, the solution was kept in a refrigerator to give microcrystals of $[Ru_2(\mu\text{-}O)(\mu\text{-}PhCOO)_2(HBpz_3)_2]$ (**1b**) in 53% yield. Anal. Calcd for $C_{32}H_{30}N_{12}O_5Ru_2B_2$: C, 43.36; H, 3.41; N, 18.96. Found: C, 43.85; H, 3.49; N, 18.76%. IR (KBr): *ν* 2484m, 1535s, 1398s, 1314s, 1209s, 1113s, 1049s, 791m, 758m, 714s, 688, 618 cm^{-1}. UV-Vis (in acetonitrile): λ_{max} (*ε*) 577 (11.85), 277 (21.29), 225 (35.90) nm (10^3 M^{-1} cm^{-1}). ^1H NMR (in $CDCl_3$): *δ* 5.51 (s, pz, 4H), 6.02 (s, pz, 4H), 7.11 (s, pz, 2H), 7.86 (s, pz, 4H), 8.71 (s, pz, 2H), 8.90 (s, pz, 2H), 7.07 (t, *m*-Ph, 4H), 7.20 (t, *p*-Ph, 2H), 7.40 (d, *o*-Ph, 4H).

$[Ru_2(\mu\text{-}OH)(\mu\text{-}RCOO)_2(HBpz_3)_2](PF_6)$ (R = Me (2a), Ph (2b)). Complex **1a**·EtOH (200 mg, 0.25 mmol) was dissolved in 50 mL of dichloromethane/methanol (1 : 1) and HPF_6 (60% water solution, 0.25 mmol) was added to the solution at room temperature. The mixture was dried over anhydrous Na_2SO_4 and was concentrated to dryness after being passed through a glass filter. The residue was crystallized from CH_2Cl_2/Et_2O to afford violet crystals of $[Ru_2(\mu\text{-}OH)(\mu\text{-}CH_3COO)_2(HBpz_3)_2](PF_6)\cdot Et_2O$ (**2a**·Et_2O) in 60% yield. Anal. Calcd for $C_{26}H_{37}N_{12}O_6Ru_2B_2PF_6$: C, 31.78; H, 3.80; N, 17.11. Found: C, 32.16; H, 3.91; N, 17.40%. IR (KBr): *ν* 2496m, 1558s, 1406s, 1316s, 1213s, 1118s, 1050s, 842s, 769, 558 cm^{-1}. UV-Vis (in acetonitrile): λ_{max} (*ε*) 544 (7.90), 394 (4.21), 338 (5.01), 252 (16.37) nm (10^3 M^{-1} cm^{-1}). ^1H NMR (in $CDCl_3$): *δ* 3.39 (s, $MeCO_2$, 6H), −5.50 (br s, pz, 4H), −1.73 (br s, pz, 2H), 2.21 (br s, pz, 2H), 4.00 (s, pz, 4H), 4.33 (s, pz, 2H), 7.31 (s, pz, 4H).

Complex **1b** (46 mg, 0.050 mmol) was treated with HPF_6 (60% water solution, 0.07 mmol) in 20 mL dichloromethane/methanol (1 : 1) at room temperature. The mixture was dried over anhydrous Na_2SO_4 and was concentrated to dryness after being passed through a glass filter. The residue was crystallized from CH_2Cl_2/Et_2O to give violet crystals of $[Ru_2(\mu\text{-}OH)(\mu\text{-}PhCOO)_2(HBpz_3)_2](PF_6)\cdot 2CH_2Cl_2$ (**2b**·$2CH_2Cl_2$) in 33% yield. Anal. Calcd for $C_{34}H_{35}N_{12}O_5Ru_2B_2PF_6Cl_4$: C, 33.97; H, 2.93; N, 13.98. Found: C, 33.44; H, 2.93; N, 13.97%. IR (KBr): *ν* 2512m, 1591m, 1537s, 1405s, 1316s, 1211s, 1119s, 1053s, 842s, 765, 720, 557 cm^{-1}. UV-Vis (in acetonitrile): λ_{max} (*ε*) 546 (6.39), 358 (5.85), 265 (22.08), 231 (41.15) nm (10^3 M^{-1} cm^{-1}). ^1H NMR (in $CDCl_3$): *δ* −0.98 (br s, pz, 4H), 2.90 (br s, pz, 2H), 5.07 (br s, pz, 4H), 5.56 (br s, pz, 2H), 5.67 (br s, pz, 2H), 7.52 (s, pz, 4H), 7.08 (br, *o*-Ph, 4H), 7.10 (br, *m*-Ph, 4H), 7.27 (br, *p*-Ph, 2H).

$[Ru_2(\mu\text{-}O)(\mu\text{-}RCOO)_2(HBpz_3)_2](PF_6)$ (R = Me (3a), Ph (3b)). Complex **1a**·EtOH (20 mg, 0.025 mmol) was treated with $(NH_4)_2Ce(NO_3)_6$ (29 mg, 0.053 mmol) and NH_4PF_6 (43 mg, 0.26 mmol) in 15 mL of acetonitrile for 2 h at room temperature. The color of the solution changed from blue to wine red. The solvent was removed under reduced pressure and the residue was extracted with CH_2Cl_2 and crystallized from CH_2Cl_2/Et_2O to give violet crystals of $[Ru_2(\mu\text{-}O)(\mu\text{-}CH_3COO)_2(HBpz_3)_2](PF_6)\cdot 0.5CH_2Cl_2$ (**3a**·$0.5CH_2Cl_2$) in 72% yield. Anal. Calcd for $C_{22.5}H_{27}N_{12}O_5Ru_2B_2ClPF_6$: C, 28.46; H, 2.87; N, 17.70. Found: C, 28.75; H, 2.98; N, 17.48%. IR (KBr): *ν* 2518m, 1506m, 1405s, 1318s, 1210s, 1120s, 1053s, 842s, 709, 558 cm^{-1}. UV-Vis (in acetonitrile): λ_{max} (*ε*) 522 (13.44), 388 (5.30), 332 (7.54), 246 (15.06) nm (10^3 M^{-1} cm^{-1}).

By a similar procedure to that used for complex **3a**, $[Ru_2(\mu\text{-}O)(\mu\text{-}PhCOO)_2(HBpz_3)_2](PF_6)\cdot 0.5CH_2Cl_2$ (**3b**·$0.5CH_2Cl_2$) was obtained in 77% yield. Anal. Calcd for $C_{32.5}H_{31}N_{12}O_5Ru_2B_2ClPF_6$: C, 36.35; H, 2.91; N, 15.65. Found: C, 37.03; H, 2.93; N, 15.12%. IR (KBr): *ν* 2519m, 1501m, 1403s, 1315s, 1207s, 1119s, 1053s, 840s, 769, 719s, 617, 503 cm^{-1}. UV-Vis (in acetonitrile): λ_{max} (*ε*) 528 (12.13), 395 (5.54), 332 (7.79), 238 (39.14) nm (10^3 M^{-1} cm^{-1}).

$[Ru(PhCO_2)(HBpz_3)(CH_3CN)_2]$ (4b). All procedures were carried out in a glove box filled with pure dinitrogen. Complex **1b** (92 mg, 0.10 mmol) was dissolved in 15 mL of acetonitrile and was stirred over *ca.* 1% sodium amalgam at room temperature for 1 h. The pale brown solution was decanted and passed through an alumina column (activated, 0.5 cm × 10 cm) eluted with acetonitrile. The eluate was concentrated and addition of hexane afforded a pale brown powder of $[Ru(PhCO_2)(HBpz_3)(CH_3CN)_2]$ (**4b**) in 63% yield. Anal. Calcd for $C_{20}H_{21}N_8O_2BRu$: C, 46.44; H, 4.09; N. 21.66. Found: C, 45.99; H, 4.16; N, 22.07%. IR (KBr): *ν* 2466m, 2258m, 1670, 1596m, 1562s, 1498m, 1402s, 1308s, 1209s, 1110s, 1043s, 795, 756, 718, 623

Table 1 Crystallographic data for **1a**·Et_2O, **2a**·Et_2O, and **5**·EtO·H_2O

	1a·Et_2O	**2a**·Et_2O	**5**·EtO·H_2O
Formula	$C_{26}H_{36}N_{12}O_6B_2Ru_2$	$C_{26}H_{37}N_{12}O_6B_2PF_6Ru_2$	$C_{36}H_{59}N_{12}O_7BRu_2$
M	836.41	982.38	984.89
Crystal system	Monoclinic	Monoclinic	Monoclinic
Space group	$P2_1/c$ (no. 14)	$P2_1/n$ (no. 14)	$P2_1/n$ (no. 14)
a/Å	14.457(3)	11.989(4)	10.826(5)
b/Å	13.068(3)	19.849(6)	22.079(3)
c/Å	18.727(2)	16.361(5)	18.589(4)
β/°	104.00(1)	104.11(2)	92.13(3)
V/Å^3	3433.0(9)	3775(1)	4440(2)
Z	4	4	4
T/°C	−117	−118	−118
D_{calcd}/g cm^{-1}	1.618	1.728	1.473
μ/cm^{-1}	9.38	9.29	7.39
R	0.039	0.035	0.048
R_w	0.047	0.042	0.050

cm^{-1}. ^{1}H NMR (in CD_3CN): δ 6.27 (br t, pz, 3H), 7.30 (d, *o*-Ph, 2H), 7.41 (t, *p*-Ph, 1H), 7.78 (br d, pz, 3H), 7.90 (br, *m*-Ph, 2H), 8.10 (br d, pz, 3H).

[Ru_2(μ-O)(μ-$CH_3COO)_2$(HB(3,5-Me_2pz)$_3$)(3,5-Me_2pz)(3,5-Me_2pzH)$_2$] (5). [$Ru_2(CH_3COO)_4Cl$] (254 mg, 0.54 mmol) and K[HB(3,5-Me_2pz)$_3$] (377 mg, 1.12 mmol) were dissolved in 15 mL of methanol and the solution was stirred at room temperature for 24 h. The color of the solution gradually changed from brown to bluish green. The reaction mixture was concentrated and chromatographed on an alumina column (10% deactivated) (2.5 cm × 15 cm) eluted with CH_2Cl_2. The blue band was collected and concentrated to dryness. The residue was crystallized from hot ethanol to give only a small quantity of crystals of [Ru_2(μ-O)(μ-$CH_3COO)_2$(HB(3,5-Me_2pz)$_3$)(3,5-Me_2pz)(3,5-Me_2pzH)$_2$]·EtOH·H_2O (**5**·EtO·H_2O), which were characterized by an X-ray crystallographic analysis.

X-Ray crystallographic analyses

Crystal data are listed in Table 1. All data were collected at low temperature on a Rigaku AFC7R diffractometer by using graphite monochromated Mo-Kα ($\lambda = 0.71069$ Å) radiation. Reflection data were corrected for Lorentz-polarization and absorption (by ψ-scan method) effects.

The structures of **1a**·Et_2O, **2a**·Et_2O, and **5**·EtO·H_2O were solved by direct methods with SIR92.[24] The coordinates of all hydrogen atoms were determined by difference Fourier syntheses for **1a**·Et_2O and **2a**·Et_2O. The O-, N-, B-bound hydrogen atoms were determined by difference Fourier syntheses and the C-bound hydrogen atoms were calculated at ideal positions with a C–H distance of 0.95 Å for **5**·EtOH·H_2O. The structures were refined with full-matrix least-square techniques on F minimizing $\Sigma w(|F_o| - |F_c|)^2$. Final refinement with anisotropic thermal parameters for all non-hydrogen atoms and isotropic ones for all hydrogen atoms converged to $R = 0.039$ and $R_w = 0.047$ ($w = 1/\sigma^2(F_o)$) for **1a**·Et_2O and to $R = 0.035$ and $R_w = 0.042$ for **2a**·Et_2O. The refinement with anisotropic thermal parameters for all non-hydrogen atoms (the hydrogen atoms were not refined) converged at $R = 0.048$ and $R_w = 0.050$ for **5**·EtOH·H_2O. Atomic scattering factors and f' and f'' for Ru, P, F, O, N, C, and B were taken from the literature.[25] All calculations were carried out on Silicon Graphics Indigo and O2 Stations with the TEXSAN Program System.[26] Perspective drawings were drawn by using ORTEP-II.[27]

CCDC reference numbers 158151–158153.

See http://www.rsc.org/suppdata/dt/b1/b101315g/ for crystallographic data in CIF or other electronic format.

EXAFS analysis

X-Ray absorption measurements around Ru K edge (21.568–23.118 keV with 780 steps) were carried out at the Photon Factory of the National Laboratory for High Energy Physics on beam line 10B using synchrotron radiation (2.5 GeV, 340–300 mA).[28] The experiments were conducted in the transmission mode on powdered samples of complexes **1**–**3** and **4b** using a Si(311) monochromator. The theoretical expression of the obtained $k^3\chi(k)$ for the case of single scattering is shown in eqn. (1),[29] where r_i, N_i, S_i, $F_i(k)$, $\Phi_i(k)$, and σ_i represent the

$$k^3\chi(k) = \Sigma_i \left(\frac{k^2 N_i}{r_i^2} S_i F_i(k) \exp(-2\sigma_i^2 k^2) \sin(2kr_i + \Phi_i(k)) \right) \quad (1)$$

interatomic distance, the coordination number, the reducing factor, the back-scattering amplitude, the phase shift, and the Debye–Waller factor, respectively, and k is the photoelectron wave vector defined as $k = [(2m/\hbar^2)(E - E_0)]^{1/2}$ ($E_0 = 22.120$ keV). The back-scattering amplitude $F_i(k)$ and the phase shift $\Phi_i(k)$ functions used were the theoretical parameters calculated by the program FEFF5.[30] Parameters, N_i, r_i, σ_i, E_0 were varied in the nonlinear least-squares refined curve fitting to the Fourier-filtered and the raw EXAFS data with fixed values of S_i. The fixed reducing factors S_i are determined by the analysis of **1a**. All calculations were performed on an Hewlett Packard Work Station Model 712/60 with the EXAFS analysis program package, REX2 (Rigaku Co. Ltd.).[31]

Results and discussion

Complexes prepared in this study, [Ru^{III}_2(μ-O)(μ-$RCOO)_2$-($HBpz_3$)$_2$] (R = Me (**1a**), Ph (**1b**)), [Ru^{III}_2(μ-OH)(μ-$RCOO)_2$-($HBpz_3$)$_2$](PF_6) (R = Me (**2a**), Ph (**2b**)), [$Ru^{III}Ru^{IV}$(μ-O)-(μ-$RCOO)_2$($HBpz_3$)$_2$](PF_6) (R = Me (**3a**), Ph (**3b**)), and [Ru^{II}(PhCOO)($HBpz_3$)(CH_3CN)$_2$] (**4b**), are summarized in Scheme 1.

Oxo-bridged diruthenium(III) complexes, [Ru_2(μ-O)(μ-$RCOO)_2$-($HBpz_3$)$_2$] (1)

Reactions of [$Ru_2(RCOO)_4Cl$] with two equivs. of potassium hydrotris(1-pyrazolyl)borate (K[$HBpz_3$]) in methanol afforded the neutral diruthenium(III) complexes, [Ru_2(μ-O)(μ-$RCOO)_2$-($HBpz_3$)$_2$] (R = Me (**1a**), Ph (**1b**)), in moderate yields (Scheme 1). The IR spectra indicated the presence of hydrotris-(1-pyrazolyl)borate and carboxylate ligands at 2484–2477 cm^{-1} (ν_{HB}) and 1550–1398 cm^{-1} (ν_{CO_2}). Complexes **1** are diamagnetic and the ^{1}H NMR spectra showed peaks for the $HBpz_3$ and RCOO units in a 1 : 1 ratio. Two unequivalent pyrazolyl rings are observed in a 2 : 1 ratio, which is in agreement with the crystal structure of **1a** as described below. In the electronic absorption spectra in acetonitrile (Fig. 1), an intense absorption band was observed around 570 nm ($\varepsilon = 13940$ M^{-1} cm^{-1}) for **1a** and 577 nm ($\varepsilon = 11850$ M^{-1} cm^{-1}) for **1b**, assignable to a

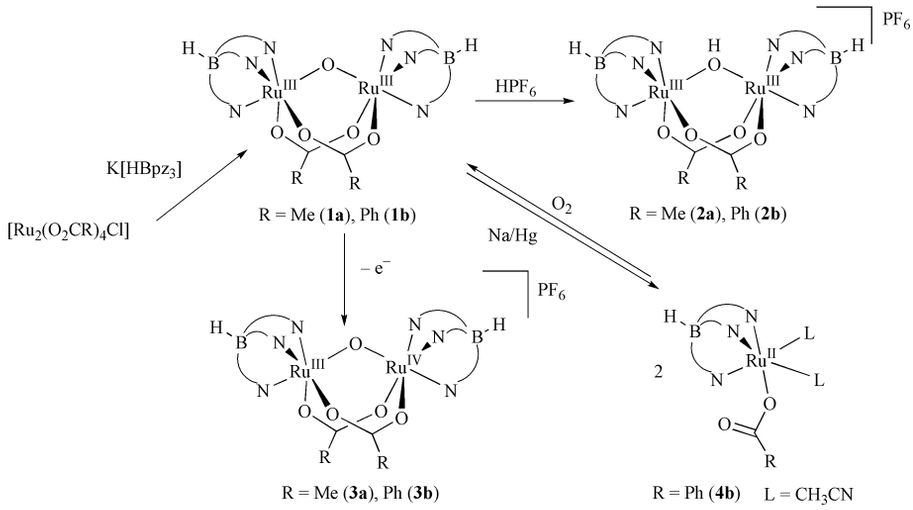

Scheme 1

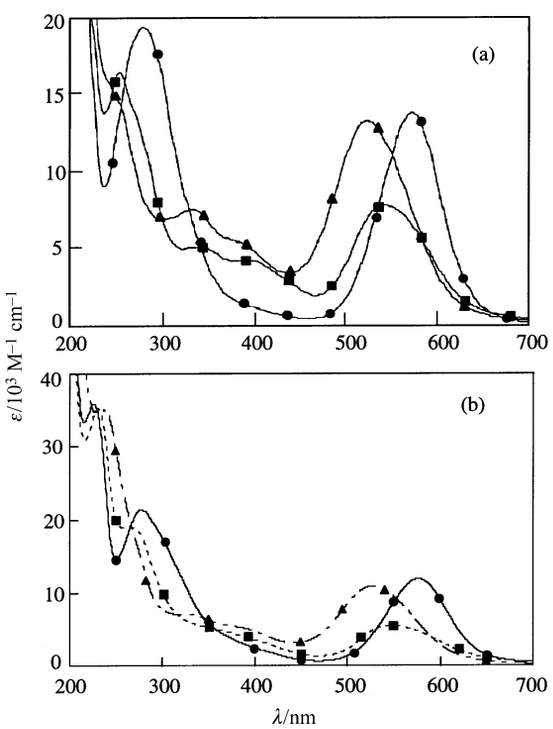

Fig. 1 (a) UV-Vis spectra of $[Ru_2(\mu\text{-}O)(\mu\text{-}CH_3COO)_2(HBpz_3)_2]$ (**1a**) (—●—), $[Ru_2(\mu\text{-}OH)(\mu\text{-}CH_3COO)_2(HBpz_3)_2](PF_6)$ (**2a**) (—■—), and $[Ru_2(\mu\text{-}O)(\mu\text{-}CH_3COO)_2(HBpz_3)_2](PF_6)$ (**3a**) (—▲—) in acetonitrile. (b) UV-Vis spectra of $[Ru_2(\mu\text{-}O)(\mu\text{-}PhCOO)_2(HBpz_3)_2]$ (**1b**) (—●—), $[Ru_2(\mu\text{-}OH)(\mu\text{-}PhCOO)_2(HBpz_3)_2](PF_6)$ (**2b**) (---■---), and $[Ru_2(\mu\text{-}O)(\mu\text{-}PhCOO)_2(HBpz_3)_2](PF_6)$ (**3b**) (–·–▲–·–) in acetonitrile.

transition between the Ru dπ and oxygen pπ orbitals of the oxo-bridged diruthenium(III) moiety.[6,7,11]

The complex **1a** has a pseudo C_s symmetry with the mirror plane passing along the Ru–O–Ru unit and consists of two Ru(III) octahedrons bridged by an oxo and two acetate ligands with two face-capping $HBpz_3^-$ ligands (Fig. 2 and Table 2). The Ru···Ru distance is 3.2544(7) Å and the Ru–O–Ru angle is 121.7(2)°. The (μ-oxo)bis(μ-acetate)diruthenium(III) core of **1a** is essentially identical to those of cationic compounds, $[Ru_2(\mu\text{-}O)(\mu\text{-}CH_3COO)_2(Me_3tacn)_2]^{2+}$ (Me_3tacn = 1,4,7-trimethyl-1,4,7-triazacyclononane),[6] $[Ru_2(\mu\text{-}O)(\mu\text{-}CH_3COO)_2(py)_6]^{2+}$,[7] $[Ru_2(\mu\text{-}O)(\mu\text{-}CH_3COO)_2(1\text{-}MeIm)_6]^{2+}$,[11] $[Ru_2(\mu\text{-}O)(\mu\text{-}CH_3COO)_2(ImH)_6]^{2+}$ (ImH = imidazole),[11] $[Ru_2(\mu\text{-}O)(\mu\text{-}CH_3COO)_2(bpy)_2(1\text{-}MeIm)_2]^{2+}$,[12] and $[Ru_2(\mu\text{-}O)(\mu\text{-}O_2P(O)(OH))_2(tpm)_6]$ (tpm = tris(1-pyrazolyl)methane).[32] The structural parameters are summarized in Table 3. The hydrotris(1-pyrazolyl)borate anions act as face-capping ligands with the usual κ^3 bonding mode, although a slight distortion due to the strong *trans* influence of the oxo group is observed with the longer distances of Ru(1)–N(11) = 2.130(4) Å and Ru(2)–N(21) = 2.118(4) Å.

When potassium hydrotris(3,5-dimethyl-1-pyrazolyl)borate ($K[HB(3,5\text{-}Me_2pz)_3]$) was used instead of $K[HBpz_3]$, the reaction of $[Ru_2(CH_3COO)_4Cl]$ proceeded slowly and the (μ-oxo)-

Table 2 Selected bond distances (Å) and angles (deg) for **1a**·Et_2O

Ru(1)···Ru(2)	3.2544(7)		
Ru(1)–O(1)	1.868(3)	Ru(1)–O(2)	2.085(3)
Ru(1)–O(4)	2.080(3)	Ru(1)–N(11)	2.130(4)
Ru(1)–N(13)	2.040(4)	Ru(1)–N(15)	2.038(4)
Ru(2)–O(1)	1.858(3)	Ru(2)–O(3)	2.072(3)
Ru(2)–O(5)	2.090(3)	Ru(2)–N(21)	2.118(4)
Ru(2)–N(23)	2.039(4)	Ru(2)–N(25)	2.042(4)
O(1)–Ru(1)–O(2)	97.3(1)	O(1)–Ru(1)–O(4)	91.9(1)
O(1)–Ru(1)–N(11)	175.5(1)	O(1)–Ru(1)–N(13)	88.4(1)
O(1)–Ru(1)–N(15)	94.0(1)	O(2)–Ru(1)–O(4)	89.3(1)
O(2)–Ru(1)–N(11)	87.1(1)	O(2)–Ru(1)–N(13)	173.9(1)
O(2)–Ru(1)–N(15)	89.9(1)	O(4)–Ru(1)–N(11)	88.6(1)
O(4)–Ru(1)–N(13)	92.8(1)	O(4)–Ru(1)–N(15)	174.1(1)
N(11)–Ru(1)–N(13)	87.1(2)	N(11)–Ru(1)–N(15)	85.4(1)
N(13)–Ru(1)–N(15)	87.5(2)	O(1)–Ru(2)–O(3)	92.0(1)
O(1)–Ru(2)–O(5)	96.8(1)	O(1)–Ru(2)–N(21)	176.3(1)
O(1)–Ru(2)–N(23)	92.4(1)	O(1)–Ru(2)–N(25)	89.8(1)
O(3)–Ru(2)–O(5)	89.9(1)	O(3)–Ru(2)–N(21)	89.1(1)
O(3)–Ru(2)–N(23)	175.4(1)	O(3)–Ru(2)–N(25)	91.8(1)
O(5)–Ru(2)–N(21)	86.6(1)	O(5)–Ru(2)–N(23)	90.8(1)
O(5)–Ru(2)–N(25)	173.1(1)	N(21)–Ru(2)–N(23)	86.4(1)
N(21)–Ru(2)–N(25)	86.7(1)	N(23)–Ru(2)–N(25)	87.0(1)
Ru(1)–O(1)–Ru(2)	121.7(2)		

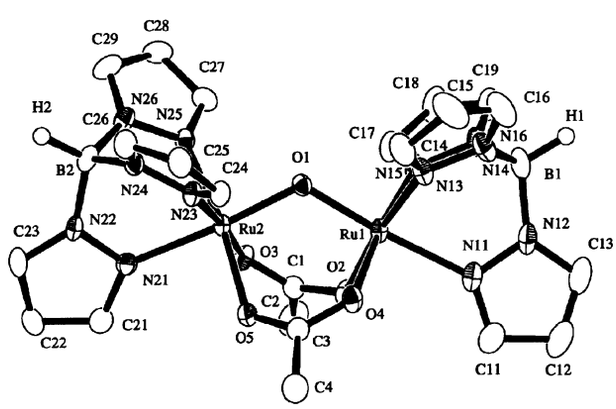

Fig. 2 ORTEP plot of $[Ru_2(\mu\text{-}O)(\mu\text{-}CH_3COO)_2(HBpz_3)_2]$ (**1a**).

Table 3 Structural parameters of diruthenium complexes containing {(μ-X)bis(μ-carboxylato)Ru_2} cores (X = O and OH)

Compound	Ru–Ru/Å	Ru–O_b [a]/Å	Ru–O_b–Ru [a]/°	Ref.
$\{Ru^{III}_2(\mu\text{-}O)(\mu\text{-}RCOO)_2\}$				
$[Ru_2(\mu\text{-}O)(\mu\text{-}CH_3COO)_2(Me_3tacn)_2]^{2+}$	3.258(1) Å	1.884(2)	119.7(2)	6
$[Ru_2(\mu\text{-}O)(\mu\text{-}CH_3COO)_2(py)_6]^{2+}$	3.251(2)	1.857 [b]	122.2(5)	7
$[Ru_2(\mu\text{-}O)(\mu\text{-}CH_3COO)_2(bpy)_2(1\text{-}MeIm)_2]^{2+}$	3.285(2)	1.882 [b]	121.5(3)	12
$[Ru_2(\mu\text{-}O)(\mu\text{-}CH_3COO)_2(1\text{-}MeIm)_6]^{2+}$	3.266(1)	1.863 [b]	122.4(4)	11
$[Ru_2(\mu\text{-}O)(\mu\text{-}CH_3COO)_2(ImH)_6]^{2+}$	3.273 [b]	1.883 [b]	120.7 [b]	11
$[Ru_2(\mu\text{-}O)(\mu\text{-}PhCOO)_2(CH_3CN)_4(PPh_3)_2]^{2+}$	3.237(1)	1.872(4)	119.7(4)	8(*a*)
$[Ru_2(\mu\text{-}O)(\mu\text{-}CH_3COO)_2(CH_3CN)_4(PPh_3)_2]^{2+}$	3.240(1)	1.866 [b]	120.6(2)	8(*b*)
$[Ru_2(\mu\text{-}O)(\mu\text{-}p\text{-}MeOC_6H_4COO)_4(PPh_3)_2]^{2+}$	3.199(1)	1.859(3)	118.7(3)	8(*a*)
$[Ru_2(\mu\text{-}O)(\mu\text{-}CH_3COO)_4(PPh_3)_2]^{2+}$	3.216(3)	1.848 [b]	121.2(9)	8(*c*)
$[Ru_2(\mu\text{-}O)(\mu\text{-}p\text{-}MeOC_6H_4COO)_2L^1_2(PPh_3)_2]^{2+}$	3.280(2)	1.887 [b]	120.7(4)	10
$[Ru_2(\mu\text{-}O)(\mu\text{-}p\text{-}MeOC_6H_4COO)_2L^2_2(PPh_3)_2]^{2+}$	3.255(3)	1.888 [b]	119.1(4)	9(*a*)
$[Ru_2(\mu\text{-}O)(\mu\text{-}CH_3COO)_2L^3_2(PPh_3)_2]^{2+}$	3.271(2)	1.881 [b]	120.9(4)	9(*b*)
$[Ru_2(\mu\text{-}O)(\mu\text{-}p\text{-}MeOC_6H_4COO)_3L^2(PPh_3)_2]^{2+}$	3.226(3)	1.870 [b]	119.2(5)	9(*c*)
$[Ru_2(\mu\text{-}O)(\mu\text{-}CH_3COO)_2(HBpz_3)_2]$ (**1a**)	3.2544(7)	1.863 [b]	121.7(2)	This work
$[Ru_2(\mu\text{-}O)(\mu\text{-}CH_3COO)_2(Tp^*)(Hpz^*)_2(pz^*)]$ (**5**)	3.3140(9)	1.875 [b]	124.2(3)	This work
$\{Ru^{III}Ru^{IV}(\mu\text{-}O)(\mu\text{-}RCOO)_2\}$				
$[Ru_2(\mu\text{-}O)(\mu\text{-}CH_3COO)_2(Me_3tacn)_2]^{3+}$	3.342(1)	1.843 [b]	130.1(3)	6
$[Ru_2(\mu\text{-}O)(\mu\text{-}CH_3COO)_2(1\text{-}MeIm)_6]^{3+}$	3.327(1)	1.810 [b]	133.6(2)	11
$\{Ru^{IV}_2(\mu\text{-}O)(\mu\text{-}RCOO)_2\}$				
$[Ru_2(\mu\text{-}O)(\mu\text{-}EtCOO)_2Cl_6]^{2-}$	3.35 [b]	1.788 [b]	138.8 [b]	14
$\{Ru^{III}_2(\mu\text{-}OH)(\mu\text{-}RCOO)_2\}$				
$[Ru_2(\mu\text{-}OH)(\mu\text{-}CH_3COO)_2(HBpz_3)_2]^+$ (**2a**)	3.4490(9)	1.959 [b]	123.4(2)	This work

[a] O_b is the bridging oxygen atom. [b] Average value. [c] Involving quadruply bridged $Ru_2(\mu\text{-}OMe)(\mu\text{-}RCOO)_3$ structure. Me_3tacn = 1,4,7-trimethyl-1,4,7-triazacyclononane, py = pyridine, 1-MeIm = 1-methylimidazole, ImH = imidazole, $L^1 = NH_2CH_2CH_2NHC(Me)NH_2$, $L^2 = NH_2CH_2CH_2NH_2$, $L^3 = Me_2NCH_2CH_2NH_2$, Tp* = hydrotris(3,5-dimethyl-1-pyrazolyl)borate, Hpz* = 3,5-dimethylpyrazole.

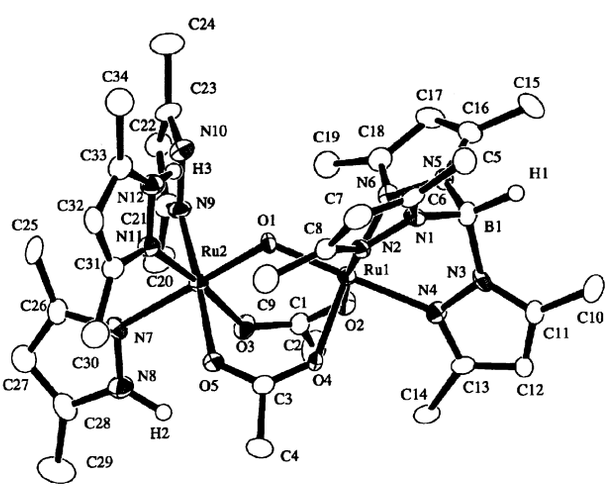

Fig. 3 ORTEP plot of $[Ru_2(\mu\text{-}O)(\mu\text{-}CH_3COO)_2(HB(3,5\text{-}Me_2pz)_3)(3,5\text{-}Me_2pz)(3,5\text{-}Me_2pzH)_2]$ (**5**).

diruthenium(III) complex, $[Ru_2(\mu\text{-}O)(\mu\text{-}CH_3COO)_2(HB(3,5\text{-}Me_2pz)_3)(3,5\text{-}Me_2pz)(3,5\text{-}Me_2pzH)_2]\cdot EtOH\cdot H_2O$ (**5**·Et_2O·H_2O), was obtained in very low yield and was characterized by X-ray crystallography. The diruthenium(III) complex $[Ru_2(\mu\text{-}O)(\mu\text{-}CH_3COO)_2(HB(3,5\text{-}Me_2pz)_3)_2]$, analogous to complex **1a**, was not formed due to steric hindrance. The more bulky hydrotris(3,5-diisopropyl-1-pyrazolyl)borate did not react with $[Ru_2(RCOO)_4Cl]$ at all. An ORTEP diagram of **5** is shown in Fig. 3 and selected bond lengths and angles are listed in Table 4. Complex **5** has an asymmetric (μ-oxo)bis(μ-acetato)-diruthenium(III) core with one terminal facial site capped by a $HB(3,5\text{-}Me_2pz)_3$ anion and the other occupied by two 3,5-dimethylpyrazol and one 3,5-dimethylpyrazolate anion derived from decomposition of hydrotris(3,5-dimethyl-1-pyrazolyl)-borate. The Ru···Ru distance is 3.3140(9) Å which is appreciably longer than that found in **1a** (Table 3). The oxo atom almost symmetrically bridges the two Ru atoms with Ru(1)–O(1) = 1.866(5) Å, Ru(2)–O(1) = 1.884(5) Å, and Ru(1)–O(1)–Ru(2) = 124.2(3)°. The pyrazole and pyrazolate groups in *cis* position to the oxo group interact *via* a hydrogen bond between the N(10) and N(12) atoms (N(10)···N(12) = 2.684(9) Å, N(10)–H(3) = 1.698(6) Å).

Table 4 Selected bond distances (Å) and angles (deg) for **5**·EtOH·H_2O

Ru(1)···Ru(2)	3.3140(9)		
Ru(1)–O(1)	1.866(5)	Ru(1)–O(2)	2.065(5)
Ru(1)–O(4)	2.091(5)	Ru(1)–N(2)	2.067(6)
Ru(1)–N(4)	2.111(7)	Ru(1)–N(6)	2.062(7)
Ru(2)–O(1)	1.884(5)	Ru(2)–O(3)	2.091(5)
Ru(2)–O(5)	2.082(5)	Ru(2)–N(7)	2.133(7)
Ru(2)–N(9)	2.075(6)	Ru(2)–N(11)	2.065(6)
O(1)–Ru(1)–O(2)	94.5(2)	O(1)–Ru(1)–O(4)	93.7(2)
O(1)–Ru(1)–N(2)	92.0(2)	O(1)–Ru(1)–N(4)	178.1(2)
O(1)–Ru(1)–N(6)	93.6(2)	O(2)–Ru(1)–O(4)	91.4(2)
O(2)–Ru(1)–N(2)	172.7(2)	O(2)–Ru(1)–N(4)	87.4(2)
O(2)–Ru(1)–N(6)	87.6(2)	O(4)–Ru(1)–N(2)	91.2(2)
O(4)–Ru(1)–N(4)	86.5(2)	O(4)–Ru(1)–N(6)	172.7(2)
N(2)–Ru(1)–N(4)	86.0(2)	N(2)–Ru(1)–N(6)	88.9(2)
N(4)–Ru(1)–N(6)	86.2(3)	O(1)–Ru(2)–O(3)	95.5(2)
O(1)–Ru(2)–O(5)	94.1(2)	O(1)–Ru(2)–N(7)	177.7(2)
O(1)–Ru(2)–N(9)	90.8(2)	O(1)–Ru(2)–N(11)	88.2(2)
O(3)–Ru(2)–O(5)	86.0(2)	O(3)–Ru(2)–N(7)	86.7(2)
O(3)–Ru(2)–N(9)	90.9(2)	O(3)–Ru(2)–N(11)	175.2(2)
O(5)–Ru(2)–N(7)	85.3(2)	O(5)–Ru(2)–N(9)	174.4(2)
O(5)–Ru(2)–N(11)	90.8(2)	N(7)–Ru(2)–N(9)	89.9(3)
N(7)–Ru(2)–N(11)	89.5(3)	N(9)–Ru(2)–N(11)	92.0(2)
Ru(1)–O(1)–Ru(2)	124.2(3)		

Hydroxo-bridged diruthenium(III) complexes, $[Ru_2(\mu\text{-}OH)(\mu\text{-}RCOO)_2(HBpz_3)_2](PF_6)$ (2)

Treatment of **1** with HPF_6 (60% in water) yielded violet crystals of $[Ru_2(\mu\text{-}OH)(\mu\text{-}RCOO)_2(HBpz_3)_2](PF_6)$ (**2a**: R = Me, 60%; **2b**: R = Ph, 33%) (Scheme 1). The IR spectra indicated the presence of $HBpz_3^-$ and RCO_2^- ligands as well as the PF_6 anion at

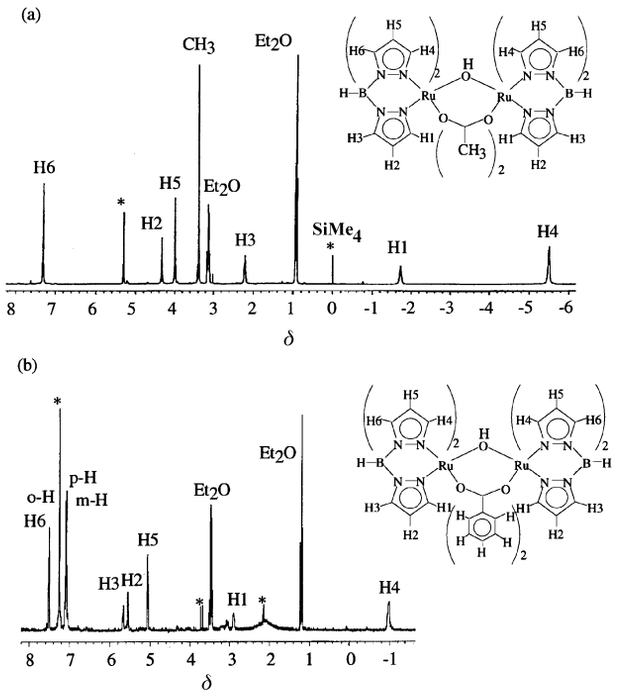

Fig. 4 ^{1}H NMR spectra of (a) $[Ru_2(\mu\text{-}OH)(\mu\text{-}CH_3COO)_2(HBpz_3)_2](PF_6)$ (**2a**) and (b) $[Ru_2(\mu\text{-}OH)(\mu\text{-}PhCOO)_2(HBpz_3)_2](PF_6)$ (**2b**) in $CDCl_3$. Impurity peaks are marked with asterisk.

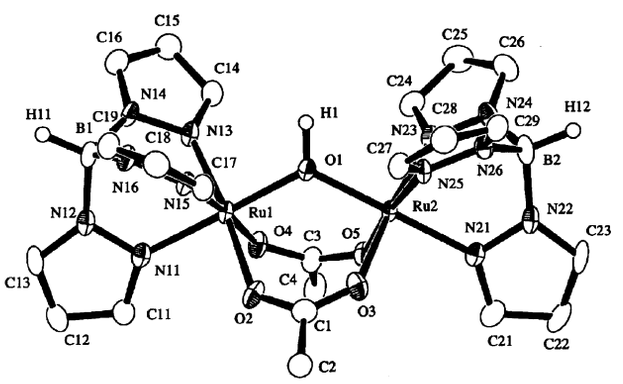

Fig. 5 ORTEP plot for the complex cation of $[Ru_2(\mu\text{-}OH)(\mu\text{-}CH_3COO)_2(HBpz_3)_2](PF_6)$ (**2a**).

842 cm^{-1}. The UV-Vis spectral patterns of **2** are quite different from those of **1**; the lowest energy bands were blue-shifted and their intensities were reduced by half (544 nm (ε = 7900 M^{-1} cm^{-1}) for **2a** and 546 nm (ε = 6390 M^{-1} cm^{-1}) for **2b**), in comparison with those of complexes **1** (Fig. 1). Similar spectral changes caused by protonation at the μ-oxo group were also reported for $[Ru_2(\mu\text{-}O)(\mu\text{-}CH_3COO)_2(Me_3tacn)_2]^{2+}$ and $[Ru_2(\mu\text{-}O)(\mu\text{-}CH_3COO)_2(1\text{-}MeIm)_6]^{2+}$.[6,11] The protonation and deprotonation proceeded reversibly in a quantitative manner by addition of TsOH to **1a** and Et_3N to **2a**, which were monitored by electronic spectral changes. The ^{1}H NMR spectra of **2** showed isotropically shifted features from δ −5.5 to 7.4 (**2a**) and δ −1.0 to 7.6 (**2b**) owing to its paramagnetism (Fig. 4). Assignments were carried out on the basis of ^{1}H–^{1}H COSY NMR spectra, which indicated that two spin sequences for the pyrazolyl rings (H1–H3 and H4–H6) existed in an integration ratio of 1 : 2. The upper-field shifted broad peaks at δ −5.5 and −1.7 (**2a**) and δ −1.0 and 2.9 (**2b**) were estimated to correspond to the 3-protons of the pz rings, H4 and H1, respectively, because they are the closest protons to the paramagnetic ruthenium centres. The extent of the paramagnetic influence in **2a** was larger than that found in **2b**.

Table 5 Selected bond distances (Å) and angles (deg) for **2a**·Et_2O

Ru(1)···Ru(2)	3.4490(9)		
Ru(1)–O(1)	1.957(3)	Ru(1)–O(2)	2.080(4)
Ru(1)–O(4)	2.065(3)	Ru(1)–N(11)	2.034(4)
Ru(1)–N(13)	2.030(4)	Ru(1)–N(15)	2.031(4)
Ru(2)–O(1)	1.960(3)	Ru(2)–O(3)	2.069(4)
Ru(2)–O(5)	2.074(3)	Ru(2)–N(21)	2.033(4)
Ru(2)–N(23)	2.040(4)	Ru(2)–N(25)	2.022(4)
O(1)–Ru(1)–O(2)	92.6(1)	O(1)–Ru(1)–O(4)	91.5(1)
O(1)–Ru(1)–N(11)	179.1(1)	O(1)–Ru(1)–N(13)	91.8(1)
O(1)–Ru(1)–N(15)	94.4(1)	O(2)–Ru(1)–O(4)	92.1(1)
O(2)–Ru(1)–N(11)	88.3(2)	O(2)–Ru(1)–N(13)	174.8(1)
O(2)–Ru(1)–N(15)	88.5(1)	O(4)–Ru(1)–N(11)	88.3(1)
O(4)–Ru(1)–N(13)	90.4(1)	O(4)–Ru(1)–N(15)	174.1(1)
N(11)–Ru(1)–N(13)	87.3(2)	N(11)–Ru(1)–N(15)	85.8(2)
N(13)–Ru(1)–N(15)	88.6(1)	O(1)–Ru(2)–O(3)	90.9(1)
O(1)–Ru(2)–O(5)	92.4(1)	O(1)–Ru(2)–N(21)	179.2(1)
O(1)–Ru(2)–N(23)	94.2(1)	O(1)–Ru(2)–N(25)	92.9(1)
O(3)–Ru(2)–O(5)	93.1(1)	O(3)–Ru(2)–N(21)	88.3(1)
O(3)–Ru(2)–N(23)	173.7(1)	O(3)–Ru(2)–N(25)	87.8(1)
O(5)–Ru(2)–N(21)	87.9(1)	O(5)–Ru(2)–N(23)	90.3(1)
O(5)–Ru(2)–N(25)	174.6(1)	N(21)–Ru(2)–N(23)	86.6(2)
N(21)–Ru(2)–N(25)	86.8(1)	N(23)–Ru(2)–N(25)	88.3(1)
Ru(1)–O(1)–Ru(2)	123.4(2)		

The complex cation of **2a** involves a (μ-OH)(μ-$CH_3COO)_2$-$Ru(III)_2$ core with two $HBpz_3$ ligands capping the facial sites (Fig. 5 and Table 5). The hydrogen atom (H(1)) of the OH group is unambiguously determined by difference Fourier synthesis. The bridging oxygen atom (O(1)) has an essentially sp^2 character, the sum of the bond angles being 359°, and the (μ-OH)Ru_2 unit takes a planar arrangement. The Ru···Ru distance of **2a** (3.4490(9) Å) is dramatically elongated in comparison with that of **1a** (3.2544(7) Å), mainly ascribable to the longer Ru–$O_{hydroxo}$ bond lengths (av. 1.955 Å) than the Ru–O_{oxo} ones (av. 1.855 Å). The Ru–O–Ru angle is 123.4(2)°, slightly expanded from 121.7(2)° in **1a**. This is the first example of (μ-hydroxo)bis(μ-carboxylato)diruthenium(III) complexes characterized in detail, whereas Wieghardt and co-workers have briefly reported preliminary data for the crystal structure of $[Ru(III)_2(\mu\text{-}OH)(\mu\text{-}CH_3COO)_2(tacn)_2]^{3+}$ (tacn = 1,4,7-triazacyclononane) (Ru···Ru = 3.472(2) Å).[6] Recently, Yamaguchi *et al.*, have reported the Ru···Ru distances for $[Ru^{III}_2(\mu\text{-}OH)(\mu\text{-}CH_3COO)_2(bpy)_2L_2]^{3+}$, determined by EXAFS analyses, as 3.54 Å (L = py) and 3.48 Å (L = 1-methylimidazole),[33] which were rather longer than the value for **2a**. It should be noted that the structural geometry of **2a** is closely similar to its iron counterpart, $[Fe^{III}_2(\mu\text{-}OH)(\mu\text{-}CH_3COO)_2(HBpz_3)_2]^+$ (Fe···Fe = 3.439(1) Å, Fe–O_{oxo} = 1.956 Å, Fe–O–Fe = 123.1(2)°).[34]

Oxo-bridged diruthenium(III, IV) complexes, $[Ru_2(\mu\text{-}O)(\mu\text{-}RCOO)_2(HBpz_3)_2](PF_6)$ (3)

When complexes **1** were oxidized by $(NH_4)_2Ce(NO_3)_6$ in the presence of NH_4PF_6, violet compounds formulated as $[Ru_2(\mu\text{-}O)(\mu\text{-}RCOO)_2(HBpz_3)_2](PF_6)$ (R = Me (**3a**), Ph (**3b**)) were obtained in good yields (Scheme 1). The elemental analyses and the IR spectra were in agreement with the formula. In the UV-Vis absorption spectra, an intense absorption band appeared at 522 nm (ε = 13440 M^{-1} cm^{-1}) for **3a** and 528 nm (ε = 12130 M^{-1} cm^{-1}) for **3b**, the energy of the absorption maximum shifting to higher energy by *ca.* 50 nm in comparison with complexes **1** (Fig. 1). Complexes **3** are paramagnetic and the ^{1}H NMR spectra were featureless. These results were analogous to those of the mixed-valence diruthenium(III, IV) complexes, $[Ru_2(\mu\text{-}O)(\mu\text{-}CH_3COO)_2(Me_3tacn)_2]^{3+}$ and $[Ru_2(\mu\text{-}O)(\mu\text{-}CH_3COO)_2(1\text{-}MeIm)_6]^{3+}$.[6,11] Since we obtained only small crystals of complexes **3** which were not suitable for X-ray crystallography, EXAFS analyses were performed to provide structural information.

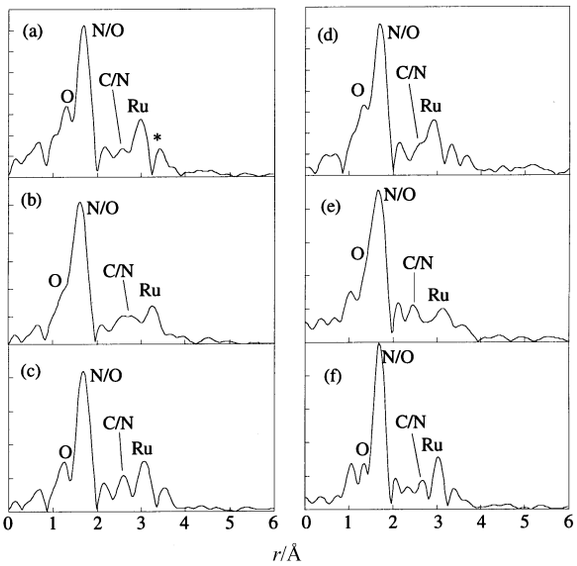

Fig. 6 Fourier transforms of the EXAFS oscillations, $k^3\chi(k)$, for (a) $[Ru_2(\mu\text{-}O)(\mu\text{-}CH_3COO)_2(HBpz_3)_2]$ (**1a**), (b) $[Ru_2(\mu\text{-}OH)(\mu\text{-}CH_3COO)_2(HBpz_3)_2](PF_6)$ (**2a**), (c) $[Ru_2(\mu\text{-}O)(\mu\text{-}CH_3COO)_2(HBpz_3)_2](PF_6)$ (**3a**), (d) $[Ru_2(\mu\text{-}O)(\mu\text{-}PhCOO)_2(HBpz_3)_2]$ (**1b**), (e) $[Ru_2(\mu\text{-}OH)(\mu\text{-}PhCOO)_2(HBpz_3)_2](PF_6)$ (**2b**), and (f) $[Ru_2(\mu\text{-}O)(\mu\text{-}PhCOO)_2(HBpz_3)_2](PF_6)$ (**3b**).

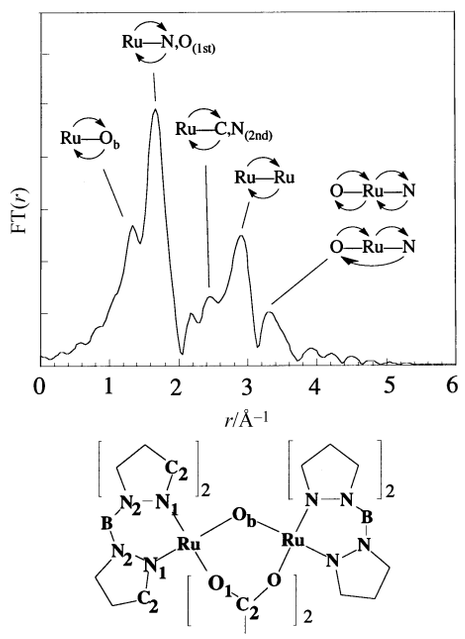

Fig. 7 Simulated FT spectrum for $[Ru_2(\mu\text{-}O)(\mu\text{-}CH_3COO)_2(HBpz_3)_2]$ (**1a**) and the peak assignments by FEFF analysis.

EXAFS analysis

X-Ray absorption spectra around Ru K edge were measured for powdered samples of complexes **1**–**3**, and Fourier transforms of EXAFS oscillation $k^3\chi(k)$ are shown in Fig. 6. In the FT spectrum of **1a** (Fig. 6a), four peaks were observed at about 1.4, 1.7, 2.6, and 3.0 Å (before phase-shift correction), which were assigned to the back-scattering contributions of the oxo atom (O_b), the O and N atoms coordinating to Ru ($O/N_{(1st)}$), the N and C atoms next to the coordinating atoms ($C/N_{(2nd)}$), and the neighboring Ru atom, respectively, on the basis of preliminary Fourier-filtered curve-fitting analyses. To confirm the assignments, effective scattering paths were calculated on the basis of the multiple scattering theory with the program FEFF6 for the X-ray crystal structure of **1a**.[35,36] The simulated FT spectrum is depicted in Fig. 7. As estimated above, the peaks around 1.4, 1.6, 2.6, and 3.0 Å are confirmed to be attributable to the two-leg effective scattering involved in the Ru–O_{oxo}, Ru–$O/N_{(1st)}$, Ru–$C/N_{(2nd)}$, and Ru–Ru combinations, respectively. In addition, the outer peaks at *ca.* 3.4 Å arose from the mixed contributions of the three- and four-leg scattering in the *trans*-[N–Ru–O] units. On the basis of these pre-assignments, the *r*-space from 0.9 Å to 3.1 Å in the FT spectrum of **1a** was back Fourier transformed into *k*-space (2–15 $Å^{-1}$) which was subject to non-linear curve-fitting analysis by using the four wave model of $k^3\chi(k) = k^3\chi(k)_O + k^3\chi(k)_{O/N} + k^3\chi(k)_{C/N} + k^3\chi(k)_{Ru}$ on the basis of the single scattering theory with theoretical $F_i(k)$ and $\Phi_i(k)$ parameters. The calculated waves, $k^3\chi(k)$, were also compared to the raw EXAFS data (Fig. 8). The structural parameters of **1a** derived from the curve-fitting analysis are listed in Table 6. Similar procedures were applied for other complexes **1b**, **2**, and **3** (Table 6).

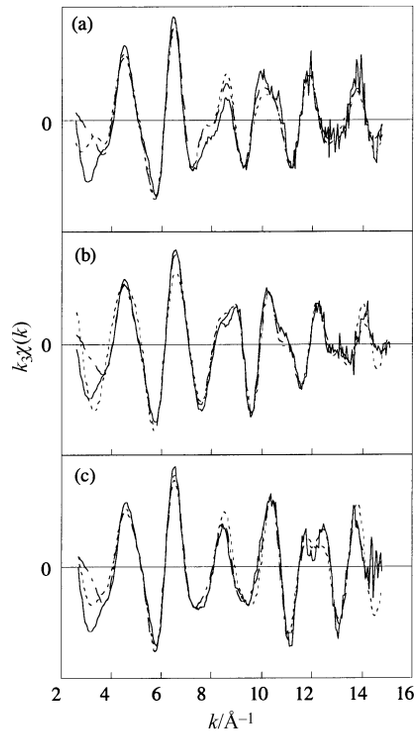

Fig. 8 Curve-fitting results, the raw $k^3\chi(k)_{raw}$ (——) and Fourier-filtered observed $k^3\chi(k)_{obsd}$ (–·–) *vs.* calculated $k^3\chi(k)_{calcd}$ (·····) for (a) $[Ru_2(\mu\text{-}O)(\mu\text{-}CH_3COO)_2(HBpz_3)_2]$ (**1a**), (b) $[Ru_2(\mu\text{-}OH)(\mu\text{-}CH_3COO)_2(HBpz_3)_2](PF_6)$ (**2a**), (c) $[Ru_2(\mu\text{-}O)(\mu\text{-}CH_3COO)_2(HBpz_3)_2](PF_6)$ (**3a**).

Whereas the parameters of **1a** and **2a** determined by EXAFS analyses were mostly comparable to those of the crystal structures, the values of the Ru–Ru distances were relatively longer than the crystallographic values: 3.29 Å (*vs.* 3.2544(9) Å) for **1a** and 3.52 Å (*vs.* 3.4490(9) Å) for **2a**. The poor Ru···Ru agreement is probably due to the complexity of the systems, overlapping shells and the multiple scattering problems from the pz rings. The Ru–Ru distance of **3a** was 3.38 Å, which is in between the values of **1a** and **2a**, and is comparable to those of the characterized diruthenium(III, IV) complexes, $[Ru_2(\mu\text{-}O)(\mu\text{-}CH_3COO)_2(Me_3tacn)_2]^{3+}$ (3.342(1) Å)[6] and $[Ru_2(\mu\text{-}O)(\mu\text{-}CH_3COO)_2(1\text{-}MeIm)_6]^{3+}$ (3.326(1) Å).[11] The EXAFS study by Yamaguchi *et al.*, also reported similar values for $[Ru_2(\mu\text{-}O)(\mu\text{-}CH_3COO)_2(bpy)_2(py)_2]^{3+}$ (3.36 Å) and $[Ru_2(\mu\text{-}O)(\mu\text{-}CH_3COO)_2(bpy)_2(1\text{-}MeIm)_2]^{3+}$ (3.36 Å), although the compounds were not isolated.[33] The Ru–Ru distances of the benzoate-bridged complexes were 3.24 Å (**1b**), 3.45 Å (**2b**), and 3.34 Å (**3b**), which were shorter by 0.4–0.7 Å than those of the corresponding acetate-bridged complexes. A similar tendency was observed in $[Ru_2(\mu\text{-}O)(RCOO)_4(PPh_3)_2]$ (R = Me (3.216(3) Å), *p*-$MeOC_6H_4$ (3.199(1) Å))[8c,10] and $[Ru_2(\mu\text{-}O)(RCOO)_2(CH_3CN)_4(PPh_3)_2]^{2+}$ (R = Me (3.240(1) Å), Ph (3.237(1) Å)).[8a,b]

Table 6 Structural parameters derived from EXAFS analyses for the ruthenium $HBpz_3$ complexes

Compound	Shell[a]	A–B[b]	N[c,h]	r/Å[d]	σ/Å[e]	R(%)
$[Ru_2(\mu\text{-}O)(\mu\text{-}O_2CCH_3)_2(HBpz_3)_2]$ (**1a**)	1st	Ru–O	1.0 (1.0)[f]	1.85 (1.863)[f]	0.017	1.1 (6.7)[g]
	2nd	Ru–N(O)	5 (5)	2.10 (2.027)	0.079	
	3rd	Ru–C(N)	8.0	3.02	0.088	
	4th	Ru–Ru	1.0 (1.0)	3.29 (3.2544)	0.080	
$[Ru_2(\mu\text{-}O)(\mu\text{-}O_2CPh)_2(HBpz_3)_2]$ (**1b**)	1st	Ru–O	0.6	1.82	0.067	5.4 (9.4)[g]
	2nd	Ru–N(O)	6.0	2.12	0.051	
	3rd	Ru–C(N)	5.1	3.02	0.041	
	4th	Ru–Ru	0.6	3.24	0.070	
$[Ru_2(\mu\text{-}OH)(\mu\text{-}O_2CCH_3)_2(HBpz_3)_2](PF_6)$ (**2a**)	1st	Ru–O	Not resolved (1.0)[f]	(1.959)[f]		3.9 (8.6)[g]
	2nd	Ru–N(O)	6.1 (5)	2.07 (2.030)	0.075	
	3rd	Ru–C(N)	10.3	3.02	0.072	
	4th	Ru–Ru	1.2 (1.0)	3.52 (3.4490)	0.078	
$[Ru_2(\mu\text{-}OH)(\mu\text{-}O_2CPh)_2(HBpz_3)_2](PF_6)$ (**2b**)	1st	Ru–O	Not resolved			9.7 (10.0)[g]
	2nd	Ru–N(O)	9.2	2.05	0.079	
	3rd	Ru–C(N)	9.1	3.02	0.064	
	4th	Ru–Ru	0.3	3.45	0.038	
$[Ru_2(\mu\text{-}O)(\mu\text{-}O_2CCH_3)_2(HBpz_3)_2](PF_6)$ (**3a**)	1st	Ru–O	1.3	1.82	0.013	3.6 (11.0)[g]
	2nd	Ru–N(O)	4.6	2.08	0.072	
	3rd	Ru–C(N)	7.7	3.04	0.078	
	4th	Ru–Ru	0.5	3.38	0.046	
$[Ru_2(\mu\text{-}O)(\mu\text{-}O_2CPh)_2(HBpz_3)_2](PF_6)$ (**3b**)	1st	Ru–O	Not resolved			11.2 (22.3)[g]
	2nd	Ru–N(O)	5.6	2.08	0.033	
	3rd	Ru–C(N)	10.3	3.01	0.067	
	4th	Ru–Ru	0.4	3.34	0.032	
$[Ru(O_2CCH_3)(HBpz_3)(CH_3CN)_2]$ (**4b**)	1st	Ru–N(O)	8.2	2.07	0.053	10.1 (20.5)[g]
	2nd	Ru–C(N)	7.9	2.99	0.062	

[a] Assignable contributions. [b] A is absorbing and B is back-scattering atoms. [c] Coordination number. Estimated errors are ±1. [d] Interatomic distance in Å. Estimated errors are ±0.03 Å for the inner shells (Ru–O, Ru–N(O)) and ±0.04 Å for the outer shells (Ru–C(N), Ru–Ru). [e] Debye–Waller factor. [f] Values in parentheses were determined by X-ray crystallography. [g] The curve-fitting analyses were performed with theoretical functions of back-scattering amplitudes and phase shifts. $R = [\Sigma(k^3\chi_o(k) - k^3\chi_c(k))^2/\Sigma(k^3\chi_o(k))^2]^{1/2}$. $\chi_o(k)$ and $\chi_c(k)$ are Fourier-filtered and calculated data, respectively. *R* values for the raw EXAFS data are given in parentheses. [h] Referenced to complex **1a**.

Electrochemical properties

The electrochemical properties of complexes **1**–**3** were analyzed by cyclic voltammetry (Fig. 9). The cyclic voltammogram (CV) of **1a** in acetonitrile containing 0.1 M $[nBu_4N][PF_6]$ as supporting electrolyte (Fig. 9a) showed two reversible oxidation waves at 0.17 V ($E_{1/2}^4$) *vs.* $Ag/AgPF_6$ with a peak-to-peak separation $\Delta E_p^4 = 90$ mV and 1.35 V ($E_{1/2}^5$) with $\Delta E_p^5 = 94$ mV, which corresponds to $[Ru^{III}_2(\mu\text{-}O)(\mu\text{-}CH_3COO)_2L_2]/[Ru^{III}Ru^{IV}(\mu\text{-}O)(\mu\text{-}CH_3COO)_2L_2]^+$ and $[Ru^{III}Ru^{IV}(\mu\text{-}O)(\mu\text{-}CH_3COO)_2L_2]^+/Ru^{IV}_2(\mu\text{-}O)(\mu\text{-}CH_3COO)_2L_2]^{2+}$ (L = $HBpz_3^-$) redox processes on the basis of coulometric analyses (Scheme 2). The extremely large half-potential separation, $\Delta E^{4,5} = |E_{1/2}^4 - E_{1/2}^5| = 1.18$ V, implies that the mixed-valent $Ru^{III}Ru^{IV}(\mu\text{-}O)$ complex is remarkably stable with the comproportionation constant K_C for $Ru^{III}_2 + Ru^{IV}_2 = 2Ru^{III}Ru^{IV}$ being 9.1×10^{19}.[16,37] In fact, a potentiostatic electrolysis of **1a** at 0.7 V consumed 1 F per dimer to afford $[Ru^{III}Ru^{IV}(\mu\text{-}O)(\mu\text{-}CH_3COO)_2L_2](PF_6)$ (**3a**), which was also prepared by the oxidation of **1a** with $(NH_4)_2Ce(NO_3)_6$ in the presence of NH_4PF_6 as described before. The CV of **1a** exhibited only one irreversible reduction wave at −1.52 V (E_{pc}^1), suggesting that a two-electron reduction of **1a** to Ru^{II}_2 species followed by a structural change of the dinuclear core is occurring. The CV of **3a** was almost identical to that of **1a**. The CV of **2a** (Fig. 9b), protonated at the oxo bridge, dramatically changed and showed two reversible reduction processes at −1.14 V ($E_{1/2}^2$) with $\Delta E_p^2 = 80$ mV and −0.45 V ($E_{1/2}^3$) with $\Delta E_p^3 = 72$ mV. The coulometric analyses indicated that they were assignable to the two-step one-electron transfer series $[Ru^{II}_2(\mu\text{-}OH)(\mu\text{-}CH_3COO)_2L_2]^- \longleftrightarrow [Ru^{II}Ru^{III}(\mu\text{-}OH)(\mu\text{-}CH_3COO)_2L_2] \longleftrightarrow [Ru^{III}_2(\mu\text{-}OH)(\mu\text{-}CH_3COO)_2L_2]^+$. The $Ru^{II}Ru^{III}$ mixed-valence species is estimated to be fairly stable from the large half-potential separation, $\Delta E^{2,3} = |E_{1/2}^2 - E_{1/2}^3| = 690$ mV ($K_C = 4.7 \times 10^{11}$). The CV at positive potential showed an extended redox couple at 0.95 V ($E_{pa}^{4'}$) and 0.25 V ($E_{pc}^{4'}$), and also showed a reversible $[Ru^{III}Ru^{IV}(\mu\text{-}O)(\mu\text{-}CH_3COO)_2L_2]^+/[Ru^{IV}_2(\mu\text{-}O)(\mu\text{-}CH_3COO)_2L_2]^{2+}$ process at 1.32 V ($E_{1/2}^5$). The characteristic process with $E_{pa}^{4'}$ and $E_{pc}^{4'}$ is assumed to involve an electrochemical (EC) mechanism as indicated in Scheme 2; one-electron oxidation of $[Ru^{III}_2(\mu\text{-}OH)(\mu\text{-}CH_3COO)_2L_2]$ and concomitant deprotonation of the hydroxo group occurred at $E_{pa}^{4'}$ to give $[Ru^{III}Ru^{IV}(\mu\text{-}O)(\mu\text{-}CH_3COO)_2L_2]^+$ which underwent one-electron reduction and protonation at $E_{pc}^{4'}$. The wave at E_{pc}^1 observed in the CV of **2a** disappeared upon addition of *p*-toluenesulfonic acid (TsOH).

The cyclic voltammograms of the benzoate-bridged complexes **1b** and **2b** exhibited similar redox processes to the acetate-bridged complexes **1a** and **2a**. The CV of **1b** showed a reversible oxidation wave at 0.21 V ($E_{1/2}^4$) with $\Delta E_p^4 = 70$ mV and two irreversible waves at 1.39 V (E_{pa}^5) and −1.46 V (E_{pc}^1) (Fig. 9c). The CV of **2b** was somewhat ambiguous due to the instability of the hydroxo-bridged structure, but in the presence of TsOH showed features comparable to those observed in **2a** (Fig. 9d), involving the proton-coupled one-electron EC process ($E_{pa}^{4'} = 1.10$ V, $E_{pc}^{4'} = 0.25$), quasi reversible one-electron oxidation ($E_{1/2}^5 = 1.38$), and two stepwise one-electron reductions at −0.41 V ($E_{1/2}^3$) with $\Delta E_p^3 = 60$ mV and −1.11 V ($E_{1/2}^2$) with $\Delta E_p^2 = 70$ mV. All potentials were slightly increased in comparison with those of the acetate-bridged complexes, owing to the electron-withdrawing effect of the benzoate ligands.

The present electrochemical study clearly demonstrates that a wide range of oxidation states, from Ru^{II}_2 to Ru^{IV}_2, are

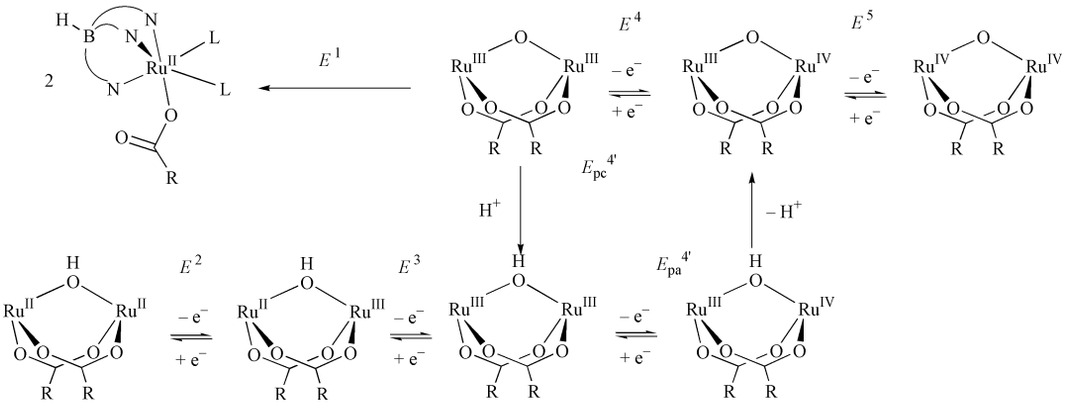

Scheme 2

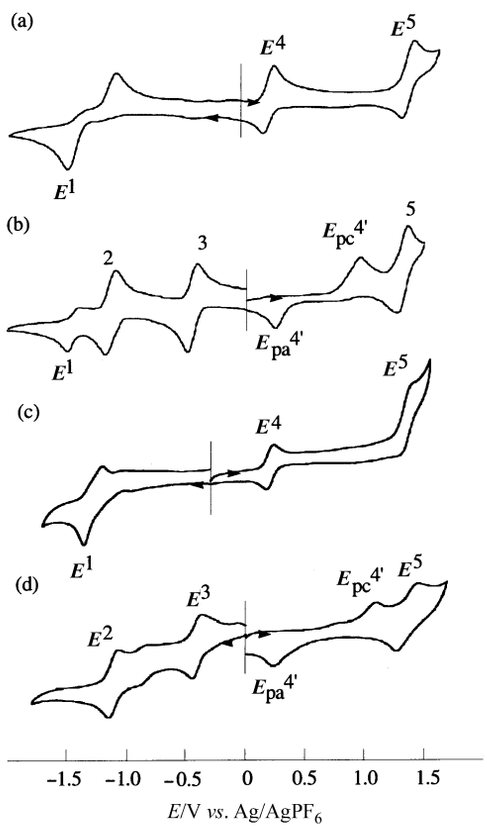

Fig. 9 Cyclic voltammograms of (a) $[Ru_2(\mu\text{-}O)(\mu\text{-}CH_3COO)_2(HBpz_3)_2]$ (**1a**), (b) $[Ru_2(\mu\text{-}OH)(\mu\text{-}CH_3COO)_2(HBpz_3)_2](PF_6)$ (**2a**), (c) $[Ru_2(\mu\text{-}O)(\mu\text{-}PhCOO)_2(HBpz_3)_2]$ (**1b**), (d) $[Ru_2(\mu\text{-}OH)(\mu\text{-}PhCOO)_2(HBpz_3)_2](PF_6)$ (**2b**) (in the presence of TsOH), in acetonitrile containing 0.1 M $[^nBu_4N][PF_6]$ with a scan rate of 100 mV s^{-1}.

accessible from the diruthenium(III) complexes **1** and **2** and that the protonation/deprotonation at the mono-atomic bridge dramatically switches the redox processes (Scheme 2). We have tried to isolate the $Ru^{II}{}_2$, $Ru^{II}Ru^{III}$, and $Ru^{IV}{}_2$ dinuclear species by electrochemical techniques but their isolation has not been successful thus far.

Reduction of oxo-bridged diruthenium(III) complexes

In order to elucidate the irreversible two-electron reduction of **1**, some attempts were carried out on the chemical reduction of the oxo-bridged diruthenium(III) complexes **1**. When complex **1b** was reduced with sodium amalgam (1%) in acetonitrile, the color of the reaction solution changed from blue to yellow and the pale brown complex formulated as $[Ru(HBpz_3)(PhCOO)(CH_3CN)_2]$ (**4b**) was isolated. A similar procedure for **1a** also afforded a pale brown solution, but the reduced species was too unstable to be isolated and characterized. The elemental and

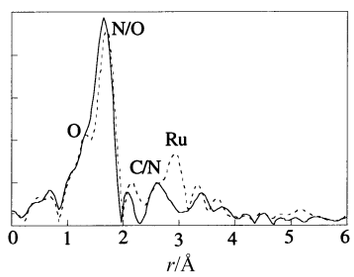

Fig. 10 Fourier transforms of the EXAFS oscillations, $k^3\chi(k)$, for $[Ru(HBpz_3)(PhCOO)(CH_3CN)_2]$ (**4b**) (——) and $[Ru_2(\mu\text{-}O)(\mu\text{-}PhCOO)_2(HBpz_3)_2]$ (**1b**) (- - -).

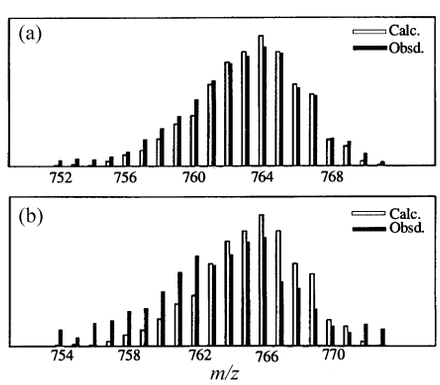

Fig. 11 MS spectra for the region of the parent ion peaks of $[Ru_2(\mu\text{-}O)(\mu\text{-}PhCOO)_2(HBpz_3)_2]$ (**1b**) derived from the reactions of **4b** with (a) $^{16}O_2$ and (b) $^{18}O_2$. The black and white bars represented the observed and calculated spectra, respectively.

IR and ^1H NMR spectral analyses suggested that $HBpz_3^-$, $PhCO_2^-$, and two CH_3CN were involved per ruthenium(II) ion. In the IR spectrum, the ν(RCOO) stretching band was shifted to higher energy at 1670 cm^{-1}, characteristic of monodentate carboxylate ligands, and in the ^1H NMR spectrum, only one kind of pyrazole ring was identified. The Fourier transform of the EXAFS data for **4b** (powdered sample) clearly demonstrated the absence of a Ru–Ru peak as observed in complex **1b** around 3.0 Å (Fig. 10). These data strongly suggested the mononuclear structure as shown in Scheme 1. Several mononuclear ruthenium(II) complexes with hydrotris(3,5-diisopropyl-1-pyrazolyl)borate ligand have recently been prepared and their oxidation by dioxygen has been examined to give ligand-oxygenated products.[38–40] In contrast, the low-valent ruthenium complex with unsubstituted $HBpz_3$ ligands has not been thoroughly studied, although the metal–metal bonded diruthenium(I) complex, $[Ru(HBpz_3)(CO)_2]_2$, has been characterized as a sole example.[41]

Complex **4b** was remarkably unstable and, upon exposure to air, the color quickly changed to blue even in the solid state.

Complex **4b** in CH_2Cl_2 readily transformed to the oxo-bridged diruthenium(III) complex **1b** by bubbling dioxygen through the solution. The same reaction was carried out with ^{18}O enriched dioxygen and the product was analyzed by FAB mass spectroscopy. The observed and calculated MS spectra for the region of parent ion peaks, corresponding to the $[Ru_2(\mu\text{-}O)(PhCOO)(HBpz_3)_2]^+$ fragment, are shown in Fig. 11. The spectrum for the product with $^{18}O_2$ increased by 2 mass units from that with $^{16}O_2$ and indicated that the oxo atom was derived from dioxygen.

Conclusion

In the present study, a series of dinuclear ruthenium complexes with hydrotris(1-pyrazolyl)borate ligands, $[Ru^{III}_2(\mu\text{-}O)(\mu\text{-}RCOO)_2(HBpz_3)_2]$ (**1**), $[Ru^{III}_2(\mu\text{-}OH)(\mu\text{-}RCOO)_2(HBpz_3)_2](PF_6)$ (**2**), and $[Ru^{III}Ru^{IV}(\mu\text{-}O)(\mu\text{-}RCOO)_2(HBpz_3)_2](PF_6)$ (**3**), were prepared (R = Me, Ph) and characterized in full detail. In particular, complex **2a** (R = Me) is the first structurally characterized example of a (μ-hydroxo)bis(μ-carboxylato)-diruthenium(III) complex. The voltammetric analyses of **1** and **2** revealed that a wide range of proton-coupled, sequential one-electron transfers, $Ru^{II}_2(\mu\text{-}OH) \leftrightarrow Ru^{II}Ru^{III}(\mu\text{-}OH) \leftrightarrow Ru^{III}_2(\mu\text{-}OH) \leftrightarrow Ru^{III}_2(\mu\text{-}O) \leftrightarrow Ru^{III}Ru^{IV}(\mu\text{-}O) \leftrightarrow Ru^{IV}_2(\mu\text{-}O)$, are accessible from the diruthenium(III) complexes. In the absence of a proton source, two-electron reduction of **1b** afforded the mononuclear Ru(II) complex, $[Ru(PhCOO)(HBpz_3)(CH_3CN)_2]$ (**4b**), which readily underwent two-electron oxidation by molecular oxygen to regenerate the oxo-bridged dimer **1b**. These results provide useful information for establishing redox-active catalytic transformations of small molecules by using diruthenium platforms.

Acknowledgements

We are grateful to Professor Yoichi Sasaki of Hokkaido University for helpful discussion. This work was partially supported by a Grant-in-Aid for Scientific Research from the Ministry of Education, Science, Culture, and Sports, Japan.

References

1 S. J. Lippard, *Angew. Chem., Int. Ed. Engl.*, 1988, **27**, 344.
2 D. M. J. Kurtz, *Chem. Rev.*, 1990, **90**, 585.
3 A. L. Feig and S. J. Lippard, *Chem. Rev.*, 1994, **94**, 759.
4 (*a*) T. Tanase, M. Kato, Y. Yamada, K. Tanaka, K. Lee, Y. Sugihara, T. Nagano and S. Yano, *Chem. Lett.*, 1994, 1853; (*b*) T. Tanase, Y. Yamada, K. Tanaka, T. Miyazu, M. Kato, K. Lee, Y. Sugihara, W. Mori, A. Ichimura, I. Kinoshita, Y. Yamamoto, M. Haga, Y. Sasaki and S. Yano, *Inorg. Chem.*, 1996, **35**, 6230.
5 Y. Mikata, N. Takeshita, T. Miyazu, Y. Miyata, T. Tanase, I. Kinoshita, A. Ichimura, W. Mori, S. Takamizawa and S. Yano, *J. Chem. Soc., Dalton Trans.*, 1998, 1969.
6 (*a*) P. Neubold, K. Wieghardt, B. Nuber and J. Weiss, *Angew. Chem., Int. Ed. Engl.*, 1988, **27**, 933; (*b*) P. Neubold, K. Wieghardt, B. Nuber and J. Weiss, *Inorg. Chem.*, 1989, **28**, 459.
7 (*a*) Y. Sasaki, M. Suzuki, A. Tokiwa, M. Ebihara, T. Yamaguchi, C. Kabuto and T. Ito, *J. Am. Chem. Soc.*, 1988, **110**, 6251; (*b*) Y. Sasaki, M. Suzuki, A. Nagasawa, A. Tokiwa, M. Ebihara, T. Yamaguchi, C. Kabuto, T. Ochi and T. Ito, *Inorg. Chem.*, 1991, **30**, 4903.
8 (*a*) B. K. Das and A. R. Chakravarty, *Inorg. Chem.*, 1990, **29**, 2078; (*b*) A. Das, B. K. Syamala and A. R. Chakravarty, *Polyhedron*, 1992, **11**, 335; (*c*) M. C. Barral, R. Jimenz-Aparicio, E. C. Royer, F. A. Urbanos, A. Monge and C. Ruiz-Valero, *Polyhedron*, 1991, **10**, 113.
9 (*a*) A. Syamala and A. R. Chakravarty, *Polyhedron*, 1993, **12**, 1545; (*b*) A. Syamala and A. R. Chakravarty, *Polyhedron*, 1994, **13**, 3079; (*c*) A. Syamala, M. Nethaji and A. R. Chakravarty, *Inorg. Chim. Acta*, 1995, **229**, 33.
10 A. Syamala and A. R. Chakravarty, *Inorg. Chem.*, 1991, **30**, 4699.
11 (*a*) C. Sudha, S. K. Mandal and A. R. Chakravarty, *Inorg. Chem.*, 1993, **32**, 3801; (*b*) C. Sudha, S. K. Mandal and A. R. Chakravarty, *Inorg. Chem.*, 1998, **37**, 270.
12 C. Sudha and A. R. Chakravarty, *J. Chem. Soc., Dalton Trans.*, 1996, 3289.
13 C. Sudha, S. K. Mandal and A. R. Chakravarty, *Inorg. Chem.*, 1994, **33**, 4878.
14 A. J. Bailey, W. P. Griffith, S. P. Marsden, A. J. P. White and D. J. Williams, *J. Chem. Soc., Dalton Trans.*, 1998, 3673.
15 W. Ruttinger and G. C. Dismukes, *Chem. Rev.*, 1997, **97**, 1 and references cited therein.
16 B. K. Das and A. R. Chakravarty, *Inorg. Chem.*, 1991, **30**, 4978.
17 (*a*) M. O. Albers, D. C. Liles, E. Singleton and J. E. Yates, *J. Organomet. Chem.*, 1984, **272**, C62; (*b*) M. O. Albers, D. C. Liles, E. Singleton and J. E. Stead, *Acta Crystallogr., Sect. C*, 1986, **42**, 46; (*c*) M. O. Albers, D. C. Liles, E. Singleton and J. E. Stead, *Acta Crystallogr., Sect. C*, 1986, **42**, 1299; (*d*) T. Arliguie, B. Chaudret, G. Chung and F. Dahan, *Organometallics*, 1991, **10**, 2973; (*e*) C. Grünwald, M. Laubender, L. Wolf and H. Werner, *J. Chem. Soc., Dalton Trans.*, 1998, 833.
18 (*a*) S. Trofimenko, *Chem. Rev.*, 1993, **93**, 943; (*b*) N. Kitajima and W. B. Tolman, *Prog. Inorg. Chem.*, 1995, **43**, 419.
19 (*a*) N. Kitajima and Y. Moro-oka, *Chem. Rev.*, 1994, **94**, 737 and references cited therein; (*b*) N. Kitajima, N. Tamura, H. Amagai, H. Fukui, Y. Moro-oka, Y. Mizutani, T. Kitagawa, R. Mathur, K. Heerwegh, C. A. Reed, C. R. Randall, L. J. Que and K. Tatsumi, *J. Am. Chem. Soc.*, 1994, **116**, 9071.
20 T. Tanase, N. Takeshita, S. Yano, I. Kinoshita and A. Ichimura, *New J. Chem.*, 1998, **22**, 927.
21 R. W. Mitchell, A. Spencer and G. Wilkinson, *J. Chem. Soc., Dalton Trans.*, 1973, 846.
22 K. D. Birinchi and A. R. Chakravarty, *Polyhedron*, 1988, **7**, 685.
23 S. Trofimenko, *J. Am. Chem. Soc.*, 1967, **22**, 6288.
24 M. C. Burla, M. Camalli, G. Cascarano, C. Giacovazzo, G. Polidori, R. Spagna and D. Viterbo, *J. Appl. Crystallogr.*, 1989, **22**, 389.
25 (*a*) D. T. Cromer, *Acta Crystallogr.*, 1965, **18**, 17; (*b*) D. T. Cromer and J. T. Waber, *International Tables for X-ray Crystallography*, Kynoch Press, Birmingham, England, 1974.
26 TEXSAN Structure Analysis Package, Molecular Structure Corporation, the Woodlands, TX, 1985.
27 C. K. Johnson, Oak Ridge National Laboratory, Oak Ridge, TN, 1976.
28 Photon Factory Activity Report, National Laboratory for High Energy Physics, Ibaraki, Japan, 1986.
29 D. E. Sayers, E. A. Stern and F. W. Lytle, *Phys. Rev. Lett.*, 1971, **27**, 1204.
30 (*a*) J. Mustre de Leon, J. J. Rehr, S. I. Zabinsky and R. C. Albers, *Phys. Rev. B*, 1991, **44**, 4146; (*b*) J. J. Rehr, R. C. Albers and S. I. Zabinsky, *Phys. Rev. Lett.*, 1992, **69**, 3397; (*c*) J. J. Rehr, J. Mustre de Leon, S. I. Zabinsky and R. C. Albers, *J. Am. Chem. Soc.*, 1991, **113**, 5135.
31 (*a*) N. Kosugi and H. Kuroda, REX, Research Centre for Spectrochemistry, the University of Tokyo, Tokyo, Japan, 1985; (*b*) REX2, Rigaku Co. Ltd., Tokyo, Japan, 1995.
32 A. Llobet, M. E. Curry, H. T. Evans and T. J. Meyer, *Inorg. Chem.*, 1989, **28**, 3131.
33 M. Valli, S. Miyata, H. Wakita, T. Yamaguchi, A. Kikuchi, K. Umakoshi, T. Imamura and Y. Sasaki, *Inorg. Chem.*, 1997, **36**, 4622.
34 W. H. Armstrong and S. J. Lippard, *J. Am. Chem. Soc.*, 1984, **106**, 4632.
35 S. I. Zabinsky, J. J. Rehr, A. Ankudinov, R. C. Albers and M. J. Eller, *Phys. Rev., B*, 1995, **52**, 2995.
36 FEFF6.01, Ab initio Multiple-Scattering X-ray Absorption Fine Structure and X-ray Absorption Near Edge Structure Code, Department of Physics, University of Washington, Seattle, WA, 1993. The effective scattering paths were calculated within the sphere of 5 Å with total Debye–Waller factor $\sigma^2 = 3.6 \times 10^{-3}$ and amplitude reduction factor $S_0^2 = 0.8$. The FEFF input file was generated by program Atoms, on the basis of the crystal structure of **1a.** The calculated EXAFS oscillations were analysed by the program REX2, (ref. 31).
37 D. E. Richardson and H. Taube, *Inorg. Chem.*, 1981, **20**, 1278.
38 Y. Takahashi, M. Akita, S. Hikichi and Y. Moro-oka, *Inorg. Chem.*, 1998, **37**, 3186.
39 Y. Takahashi, S. Hikichi, M. Akita and Y. Moro-oka, *Organometallics*, 1999, **18**, 2571.
40 Y. Takahashi, S. Hikichi, M. Akita and Y. Moro-oka, *Chem. Commun.*, 1999, 1491.
41 M. M. de V. Steyn, E. Singleton, S. Hietkamp and D. C. Liles, *J. Chem. Soc., Dalton Trans.*, 1990, 2991.